

## Comments

1. *Please provide degree or qualification for this author?* Done.
2. *Please confirm target journal?* To be determined.
3. *Authors please validate affiliations.* Done.
4. *Authors please validate address and details.* Done. Changed to current address.
5. *Please provide [fax number].* I don't have one.
6. *For how long?* The Vertex people should have this information.
7. *These references have not been provided. Please provide references.* These are fine.
8. *Please confirm this is correct.* The Vertex people should have this information.
9. *What were the number of patients? Was it 8 as specified in the abstract?* Yes, that was the number of subjects given to me to be used for the analysis.
10. *What is the treatment? According to ref 25 it is ivacaftor? Should this be stated?* This should be clarified with the Vertex people.
11. *The equations listed here are cut and pasted from a pdf document of the manuscript. Please validate these are correct? Do the authors have a cleaner version of these equations we could insert?* Done.
12. *Please also confirm that any of the equation symbols within the text are accurate (font, etc).* Done.
13. *The equations listed here are cut and pasted from a pdf document of the manuscript. Please validate these are correct? Do the authors have a cleaner version of these equations we could insert?* See above.
14. *The equations listed here are cut and pasted from a pdf document of the manuscript. Please validate these are correct? Do the authors have a cleaner version of these equations we could insert?* See above.
15. *The equations listed here are cut and pasted from a pdf document of the manuscript. Please validate these are correct? Do the authors have a cleaner version of these equations we could insert?* See above.
16. *Please indicate any potential financial conflicts related to this manuscript, such as: advisory board, paid consultant, honoraria, research grants received by you or your affiliation, speakers' bureau, owning stock in company, or employment; include funding source for each disclosure.* To be done.

# **Voxel-Based Longitudinal Analysis of Pulmonary Ventilation Magnetic Resonance Imaging**

Nicholas J. Tustison, DSc,<sup>1</sup> Benjamin Contrella, MD,<sup>1</sup> Talissa A. Altes, MD,<sup>2</sup> Brian B. Avants, PhD,<sup>3</sup> Eduard E. de Lange, MD,<sup>1</sup> John P. Mugler, III, PhD<sup>1</sup>

1. Department of Radiology and Medical Imaging, University of Virginia, Charlottesville, Virginia, USA
2. Department of Radiology, University of Missouri, Columbia, Missouri, USA
3. Penn Image Computing and Science Laboratory, University of Pennsylvania, Philadelphia, Pennsylvania, USA

## **Address for correspondence:**

Nicholas J. Tustison  
4173 Cardamon Circle  
Corona, CA 92883  
Phone: 540-383-2719  
E-mail: [ntustison@virginia.edu](mailto:ntustison@virginia.edu)

**Funding disclosure:** This study was sponsored by Vertex Pharmaceuticals Incorporated. Editorial support was provided by Infusion Communications, Haddam, CT and was funded by Vertex Pharmaceuticals Incorporated. No author received an honorarium or other form of financial support related to the development of this manuscript.

## **Abstract**

**Purpose:** Propose a methodologic framework for quantitative assessment of longitudinal pulmonary ventilation image data using hyperpolarized helium-3 ( ${}^3\text{He}$ ) for magnetic resonance imaging (MRI), including novel image processing and statistical analysis procedures for generating localized correlation maps based on effect(s) of interest.

**Methods:** Eight patients with cystic fibrosis were imaged using simultaneous hyperpolarized  ${}^3\text{He}$  and conventional  ${}^1\text{H}$  MRI every 2 weeks for 5 total time points in an experimental drug therapy study. To quantify patient-specific local treatment effects, multivariate (ie,  ${}^1\text{H}/{}^3\text{He}$ ) patient-specific atlases were constructed directly from longitudinal data. Probabilistic segmentation of the four dimensional (4-D) longitudinal image volume was used to yield normalized expected ventilation intensity values. Subsequent voxelwise regression analysis was used to determine local coherence with the proposed treatment effect hypothesis.

**Results:** Image maps were generated in the template space for each patient, showing areas of positive and negative correlation. Summing of respective regional volumes provided estimates of global effects of drug therapy, whereas the correlation image maps provided complementary information regarding local effects.

**Conclusion:** Using the proposed framework facilitates longitudinal assessment of pulmonary ventilation images. The proposed image analysis work flow appropriately modulates image data for subsequent statistical analysis yielding correlation maps that provide important regional information.

**Keywords:** cystic fibrosis; helium; respiratory function tests; magnetic resonance imaging (MRI)

## Introduction

Because of the heterogeneous nature of pathologic lung processes, studies of disease progression and treatment are complex. Longitudinal studies are advantageous in that normal between-patient variability is minimized. However, many of the longitudinal pulmonary studies conducted to date have been restricted to whole-lung spirometry assessments for evaluation of lung function, with imaging being rapidly adopted owing to its increased spatial sensitivity.

Spirometry is the standard protocol for evaluating lung function because of its low cost, noninvasive nature, and wide availability. Longitudinal spirometry studies have explored such respiratory pathologies as the effects of smoking [1, 2], asthma [3], pollution [4], allergen skin test reactivity [5], systemic sclerosis [6], coal mining [7], asbestos exposure [8], and respiratory syndromes [9].

Two major drawbacks of spirometry, however, are its inability to characterize the spatial distribution of ventilation and its insensitivity to changes in the lungs over short periods of time, thus motivating the development of imaging technology [10] that can be used independently or in conjunction with spirometry. Computed tomography (CT) has been used extensively to monitor disease progression and treatment response in chronic obstructive pulmonary disease (COPD) [11] and investigate the progression of emphysema in patients with COPD and alpha-1 antitrypsin deficiency [12]. Other longitudinal studies have assessed the correlation between CT measurements in the lungs of smokers and forced expiratory volume in 1 second (FEV1) [13], investigated CT densitometry to detect emphysema progression in patients with alpha-1 antitrypsin deficiency [14, 15], evaluated the impact of exacerbations and other factors on COPD progression through CT measurements [16, 17], and used high-resolution CT to assess smoking-induced lung density changes [18].

More recently, studies have shown that hyperpolarized helium-3 (<sup>3</sup>He) magnetic resonance imaging (MRI) has great potential to visualize ventilation defects in the lungs [19], with additional potential for computational analysis [20–22]. Several advantages are encouraging for the use of <sup>3</sup>He MRI over CT. For example, a recent study of pulmonary function as assessed by FEV1 and diffusing capacity of the lung for carbon monoxide found a stronger correlation between pulmonary function and <sup>3</sup>He MRI compared with pulmonary function and CT [23]. Although <sup>3</sup>He MRI longitudinal studies are not as numerous, they have shown great potential, as exemplified by Kirby et al, who investigated COPD progression in ex-smokers compared with healthy volunteers [24].

In order to perform analysis on <sup>3</sup>He MRI longitudinal data, the images have to first be spatially normalized to a common reference space, also known as a template or atlas. Such templates are common in the neuroimaging community, although they are found less frequently in the pulmonary research literature. One of the earliest

and most widely used templates was the Talairach atlas, created by Dr. Jean Talairach (a French neurosurgeon), who identified landmarks on the postmortem histologic sections of a 60-year-old French woman to define a universal, stereotactic cerebral space. The utility of a standardized anatomical coordinate system has prompted additional work, such as the publicly available Montreal Neurological Institute brain template [25], which is an average of hundreds of adult brain MR images all registered to the Talairach atlas. Following template construction, statistical analyses can be applied so that biological processes, such as the magnitude of a local neuroresponse to a prescribed stimuli, can be assessed [26].

In this article, a similar approach to that described in the neuroimaging example above, was applied to a novel study of patients with cystic fibrosis (CF) treated with a modulator of the mutational defect in CF. Clinical findings of improved lung ventilation with treatment were published in this cohort with CF based on hyperpolarized  $^3\text{He}$  gas imaging [27]. These data are summarized here to illustrate the innovative longitudinal aspects of this pulmonary analysis; the images were initially brought into anatomical alignment via a robust template building strategy, and then voxelwise regression over the time course was used to determine correlative regions with the simplified treatment hypothesis.

## Methods

### Cystic Fibrosis Treatment Image Data

Hyperpolarized  $^3\text{He}$  MRI was evaluated as a clinical outcome measure in a single blind, placebo-controlled, Phase 2 investigational CF trial ([www.clinicaltrials.gov](http://www.clinicaltrials.gov) identifier: NCT01161537). Patients or parents/guardians provided written informed consent, and patients younger than 18 years provided assent. The study protocol, informed consent, and other necessary documents were approved by an independent ethics committee or institutional review board for each study site before initiation of the study. This study was conducted in accordance with Good Clinical Practice (GCP) as described in the International Conference on Harmonization (ICH) Guideline E6, Good Clinical Practice, Consolidated Guidance (April 1996). The ICH GCP guideline is consistent with the World Medical Assembly Declaration of Helsinki.

The eight patients used in this analysis were aged 12 years and older with CF, with a G551D mutation on at least one allele and a percent predicted FEV1 of at least 40. Patients underwent spirometry and hyperpolarized  $^3\text{He}$  MRI every 2 weeks for 8 weeks (days 0, 14, 28, 42, and 56). Drug dosing consisted of a placebo lead-in from days 0 to 14 and treatment from days 14 to 42 (28 days), followed by a placebo washout period from days 42 to 56 (14 days).

## **Image Acquisition**

The  $^3\text{He}$  gas was polarized using a prototype commercial system (Magnetic Imaging Technologies Inc.; Durham, NC, USA), and polarizations between 20% and 40% were achieved. For each  $^3\text{He}$  MR acquisition, a 1- or 2-liter plastic bag (Jensen Inert Products; Coral Springs, FL, USA) was filled with 300 cc to 600 cc of hyperpolarized  $^3\text{He}$  and enough nitrogen to total approximately one third of the patient's forced vital capacity (FVC). The patient inhaled the hyperpolarized  $^3\text{He}$  through a small plastic tube attached to the bag containing the gas. Three-dimensional (3-D) image sets of the lung utilizing  $^3\text{He}$  MRI and MRI using hydrogen proton signals ( $^1\text{H}$ ) were acquired during a single breath hold, using a 1.5T whole-body MRI system (Avanto; Siemens Healthcare, Malvern, PA, USA) and a linearly polarized transmit/receive radiofrequency coil tuned to the  $^3\text{He}$  frequency (Rapid Biomedical; Rimpar, Germany). The 3-D true fast imaging with steady-state free precession (TrueFISP)  $^3\text{He}$  and  $^1\text{H}$  MRI acquisitions comprised the following parameters: repetition time (TR)/echo time (TE) 1.9/0.8 ms ( $^3\text{He}$ ) or 1.8/0.7 ms ( $^1\text{H}$ ), flip angle 9 degrees, and isotropic 3.9-mm spatial resolution. Elliptical k-space sampling and partial Fourier were used for both methods, resulting in a total breath-hold time of approximately 12 seconds.

## **Image Analysis**

Analysis of longitudinal data (i.e., the time points) comprises the following basic steps: multimodal atlas construction for each patient, intensity normalization and bias correction across all time points, four-dimensional (4-D) ventilation-based segmentation, and voxelwise regression analysis, with the simplified hypothesis treatment effect. Each step of the 4-D work flow is detailed below. All software described in this work is available as an open source from the Advanced Normalization Tools (ANTs) repository ([www.picsl.upenn.edu/ANTs](http://www.picsl.upenn.edu/ANTs)).

## **Multivariate Template Construction**

Patient-specific templates were generated directly from the image data. Using the  $^3\text{He}$  and  $^1\text{H}$  data for each of the 5 time points as input, generation of the patient-specific template can be intuitively understood as iterating between averaging the current set of aligned images to create an estimate of the template, then to registering the images to that template estimate (and repeating for a given number of iterations). More technically, the symmetric normalization pairwise registration algorithm and an optimized Laplacian sharpening/averaging of the template estimate form the core of what is denoted as the symmetric group normalization algorithm for template construction. Given the set of 5 time-point  $^1\text{H}/^3\text{He}$  aligned image pairs from a single patient, denoted as  $\{I_1^{1H}, I_1^{3He}, \dots, I_5^{1H}, I_5^{3He}\}$ , template generation involved finding the following: the set of paired diffeomorphic transformations,  $\{(\phi_1, \phi_1^{-1}), \dots, (\phi_5, \phi_5^{-1})\}$ ; the optimal multimodal template appearance,  $J^{1H}$  and  $J^{3He}$ ; and the corresponding coordinate system,  $\Psi(x)$ , which minimizes the following cost function:

$$\sum_{m=1}^5 \left[ D(\Psi(x), \phi_1^m(x, 1)) + \Pi_1 \left( I_m^{1H}(\phi_2^m(x, 0.5)), J^{1H}(\phi_1^m(x, 0.5)) \right) + \Pi_2 \left( I_m^{3He}(\phi_2^m(x, 0.5)), J^{3He}(\phi_1^m(x, 0.5)) \right) \right]$$

wherein  $D$  is the diffeomorphic shape distance,

$$D(\phi(x, 0), \phi(x, 1)) = \int_0^1 \|v(x, t)\|_L dt,$$

(dependent on the choice of linear operator,  $L$ , and  $v$  is the velocity field), and

$$v(\phi(x, t)) = \frac{d\phi(x, t)}{dt}, \quad \phi(x, 0) = x.$$

wherein  $\Pi$  is the choice of similarity metric, calculated in the virtual domain midway between each individual modality image and the current estimate of the corresponding template. Diffeomorphic transformations are differentiable mappings with differentiable inverses. In the context of image registration, diffeomorphic transformations ensure the existence of biologically plausible inverse mappings whereby a topology-preserving mapping from image  $I$  to  $J$  is also accompanied by a topology-preserving mapping from image  $J$  to  $I$ .

Atlas generation for each patient produced patient-specific  ${}^1\text{H}$  and  ${}^3\text{He}$  template images constituting a mean shape or appearance model of the image data for all 5 time points. In addition, each time point image was spatially normalized to the template space. These aligned data were subsequently bias field corrected and intensity normalized in preparation for 4-D segmentation (described in the next section).

### **Longitudinal Ventilation-Based Segmentation**

Preprocessing of images included suppression of inhomogeneity artifacts through the application of the N4 bias correction algorithm [28] to each individual image. This step was followed by intensity normalization, wherein the intensities of all 5 time point images were normalized to a single intensity range. Using the algorithm of Nyul et al. [28], the intensity range in each image (denoted as the “source”) from time points 2 through 5 was matched to the intensity range in the image of time point 1 (denoted as the “reference”) by selecting 5 histogram match points distributed evenly across the intensity range in both images. Each match point in the “source” histogram was assigned the intensity value of the corresponding “target” point, with linear scaling performed between match points. Only 5 match points were employed, to avoid excessive intensity distortion.

Following intensity correction and normalization, the image volumes from each time point were collated into a single spatio-temporal image, which was then segmented into 4 ventilation classes using the Atropos segmentation tool. The application of Atropos to pulmonary ventilation images was described in detail by Tustison

et al. [21]. Briefly, an expectation-maximization algorithm was used to optimize the class membership of each voxel, while a Markov random field priori was used to modulate such optimization by taking into account neighboring voxel class membership. For this study, a pixel was described by 1 of 4 categories representing degree of ventilation.

Extension to 4-D was straightforward, with the optimization being practically identical to the 3-D case. The only variation was the determination of how much the neighboring pixels in time should be taken into account. Based on preliminary work, it was determined that omitting any temporal neighbor considerations produced the best results, and this approach minimized the bias in the longitudinal analysis by not favoring a static treatment effect model.

### **Statistical Analysis**

Output of the 4-D segmentation process included the posterior probability images that indicated the probability that a particular pixel belongs to a particular ventilation category. These posterior probability images were used to produce a standard ventilation scale for each image. These scaled, expected ventilation,  $EV$ , images were calculated as follows:

$$EV(x) = \sum_{m=1}^M m \times \Pr(m|I(x))$$

wherein  $M$  is the total number of labels (as described above, we used the label set  $\{1, 2, 3, 4\}$  to describe the ventilation classes), and  $\Pr(m|I(x))$  was the posterior probability at spatial location  $x$  (i.e., the probability that voxel  $x$  has label  $m$ , given its intensity value  $I(x)$ ).

To account for any residual registration misalignments, the expected ventilation maps were smoothed prior to voxelwise regression. Correlation was then performed longitudinally at each voxel with the simplified treatment hypothesis.

## **Results**

Eight patients completed the study. For every patient, a template was created from the  ${}^3\text{He}$  and  ${}^1\text{H}$  data from each of the 5 time points to provide a normalized patient-specific space for subsequent statistical analysis of the longitudinal data. The template construction algorithm described by Avants et al. [29] normally related to T1-weighted brain data, was applied to the pulmonary data. The simultaneous acquisition of the  ${}^3\text{He}$  and  ${}^1\text{H}$  MR images allowed multimodal processing [30] in which both modalities were used to coordinate the data processing to simultaneously produce  ${}^3\text{He}$  and  ${}^1\text{H}$  templates. This process is illustrated in Figure 1 for a single patient. The alignment results of the simultaneous acquisition are shown by overlaying the faux color-rendered  ${}^3\text{He}$

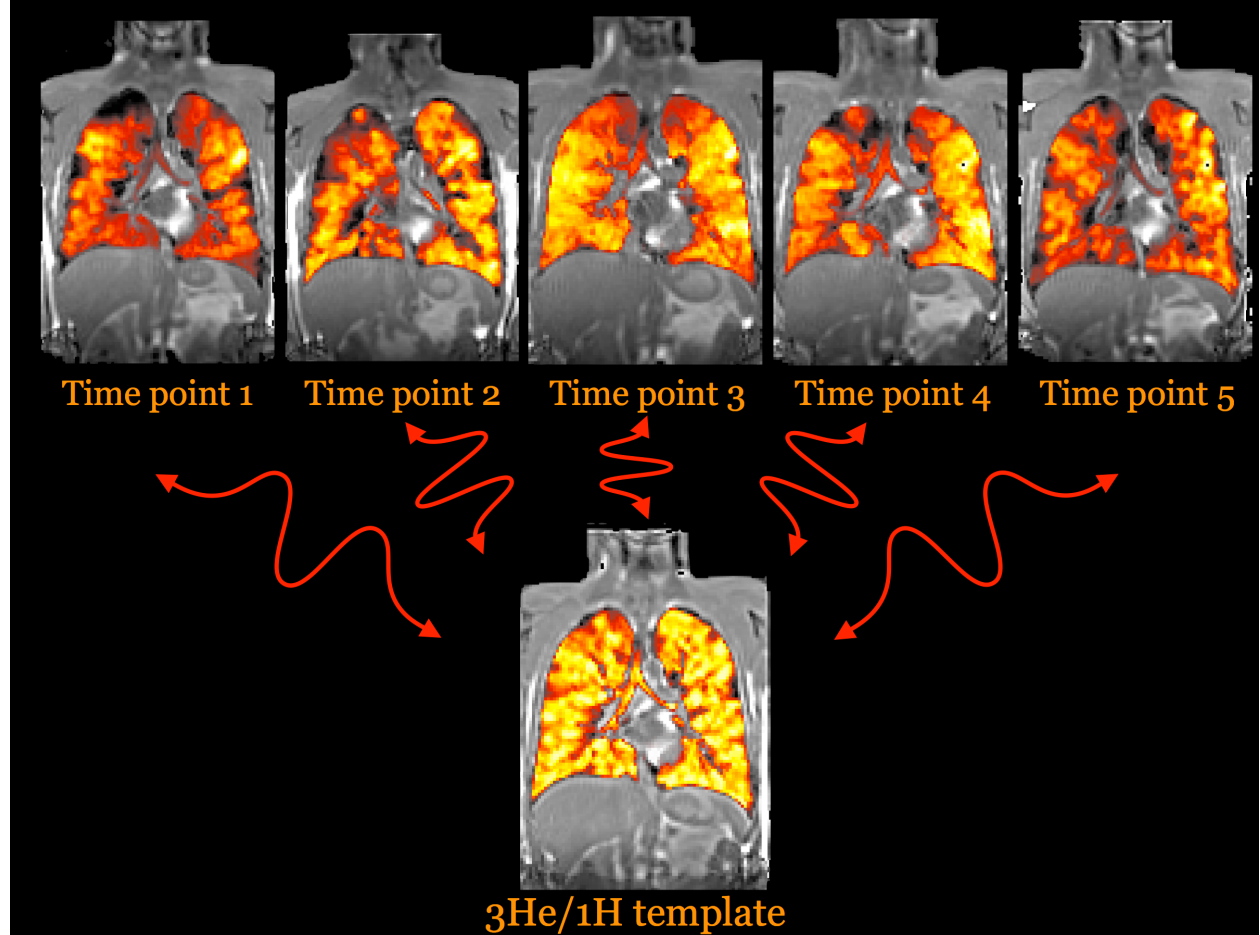


**Figure 1:** Multivariate template construction using both <sup>3</sup>He and <sup>1</sup>H images. To create a normalized patient-specific space for statistical analysis of the longitudinal data, a template was created from the <sup>3</sup>He and <sup>1</sup>H data from each of the 5 time points. Aligned results are shown of the simultaneous acquisition by superimposing the faux color-rendered <sup>3</sup>He image over the grayscale <sup>1</sup>H image. The template was created iteratively wherein the algorithm alternated between averaging the registered images then registering each time point to the average image (i.e., template estimate).

image over the grayscale 1H image. The template was generated iteratively wherein the algorithm alternated between averaging the registered images then registering each time point to the average image (i.e., template estimate).

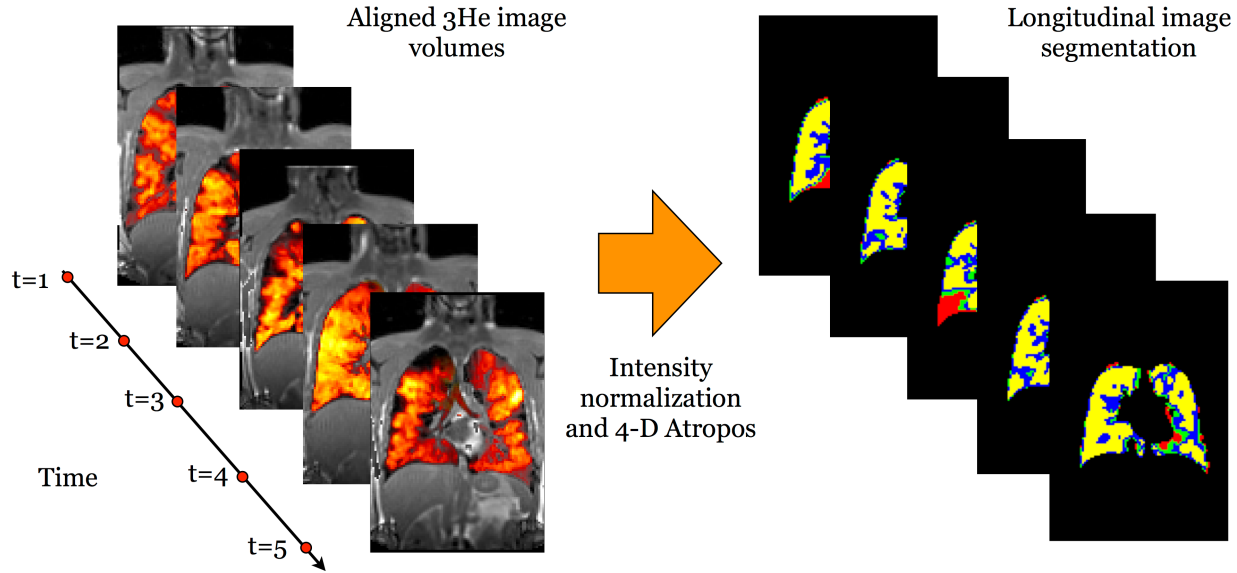


**Figure 2:** Four-dimensional (4-D) segmentation of the aligned 3-D image volumes. After N4 inhomogeneity correction was applied to the 5 time point image volumes, each of the corrected 3-D images from time points 2 through 5 were intensity normalized to the first time point. The 5 resulting corrected and normalized 3-D images were subsequently collated into a single, 4-D spatio-temporal image, which was segmented into 4 classes using Atropos segmentation.

After N4 inhomogeneity correction was applied to each of the 5 time point image volumes, the individual corrected 3-D images from time points 2 through 5 were intensity normalized to the first time point. The 5 resulting corrected and normalized 3-D images were then collated into a single, 4-D spatio-temporal image, which was segmented using Atropos into 4 classes (Figure 2).

Following inhomogeneity correction and segmentation of the longitudinal image volumes for each of the 8 patients, expected ventilation image maps were created from the segmentation output using Equation 4. Images were then smoothed, as demonstrated in Figure 3, to account for any registration inaccuracies. A volumetric correlation map was generated for each of the 8 patients by identifying positively and negatively correlated regions satisfying  $|r| \geq 0.5$  and  $|EV_3 - EV_2| \geq 0.1$ , wherein  $r$  is Pearson's correlation coefficient, and  $EV_3$  and  $EV_2$  are the expected ventilation values at time points 3 and 2, respectively. In the relevant correlation map for each patient (Figure 4), orange and blue differentiate the positively and negatively correlated regions, respectively. Subsequent analyses included the calculation of positively and negatively correlated subvolumes in

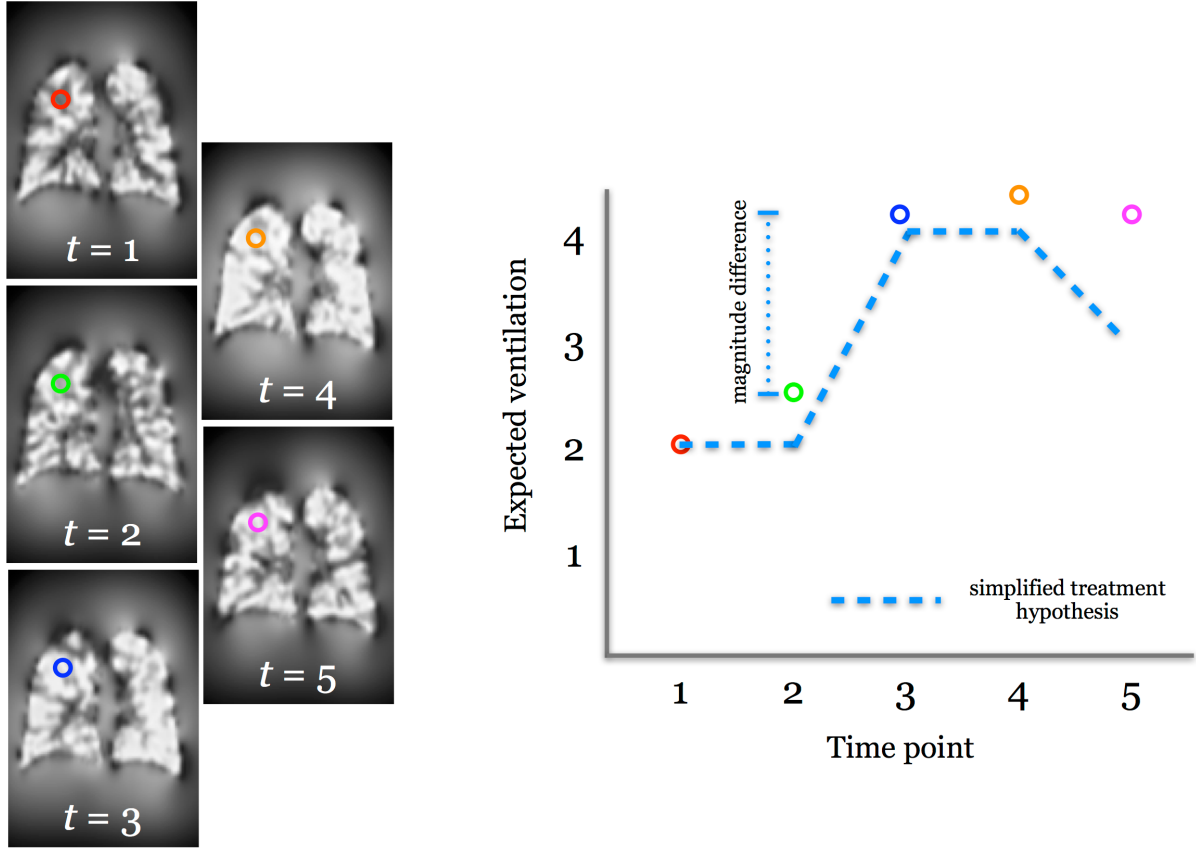


**Figure 3:** Voxelwise regression analysis to determine image-based response to treatment. Treatment effects are expected to follow the simplified treatment hypothesis illustrated with the dashed blue line in the plot on the right. To explore how the longitudinal change in expected ventilation follows this treatment hypothesis with image data, the aligned expected ventilation maps were smoothed (to account for potential voxelwise misalignments), and regression of voxelwise intensities with the simplified treatment hypothesis was quantified.

the template space (Table 1) to provide a global synthesis of the region-based quantities. Furthermore, regions of the lung that improved with treatment could be identified in a patient-specific manner. For example, in Figure 5, a view of the left lung of patient 3 can be seen, showing only positively correlated regions. The arrows designate the lobar fissure, revealing a predominant upper lobe treatment effect in this particular patient.

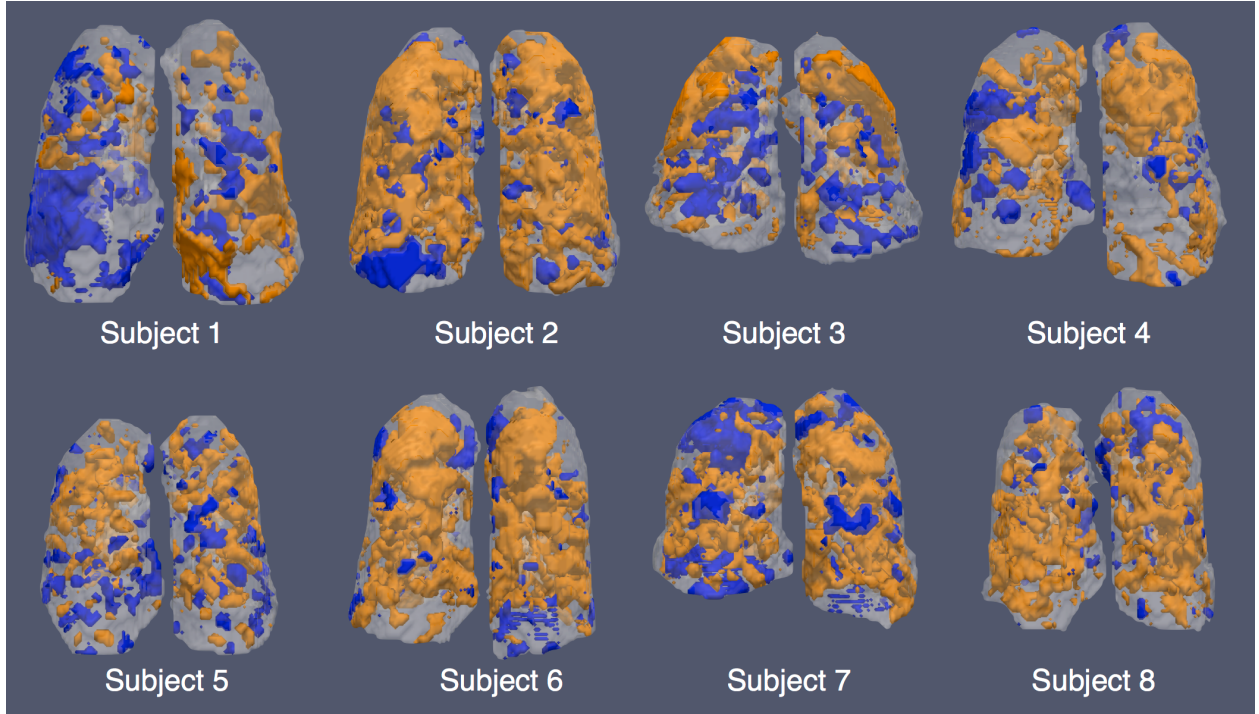


**Figure 4:** Signed magnitude maps for all 8 patients showing regions of significant positive (orange) and negative (blue) correlations, i.e., regions that responded according to the treatment hypothesis appear in orange, whereas regions exhibiting inverse correlations appear in blue. The rendered regions had absolute correlation values greater than or equal to 0.5 and an effect size (i.e., the difference in expected ventilation between time points  $t = 2$  and  $t = 3$ ) greater than or equal to 1.0.

## Discussion

Increased use of imaging for pulmonary longitudinal studies will require computational techniques to quantify and visualize spatial data in both local and global terms. A framework has been presented here for data preparation in future single-patient longitudinal studies whereby multivariate template construction results in longitudinal alignment. Results were presented using a unique cohort of patients with CF imaged at 5 discrete time points while undergoing various stages of drug treatment.

For the analysis of this work, patient-specific templates were generated directly from the image data. Given the variability in lung shape across populations and the lack of publicly available lung atlases, generating

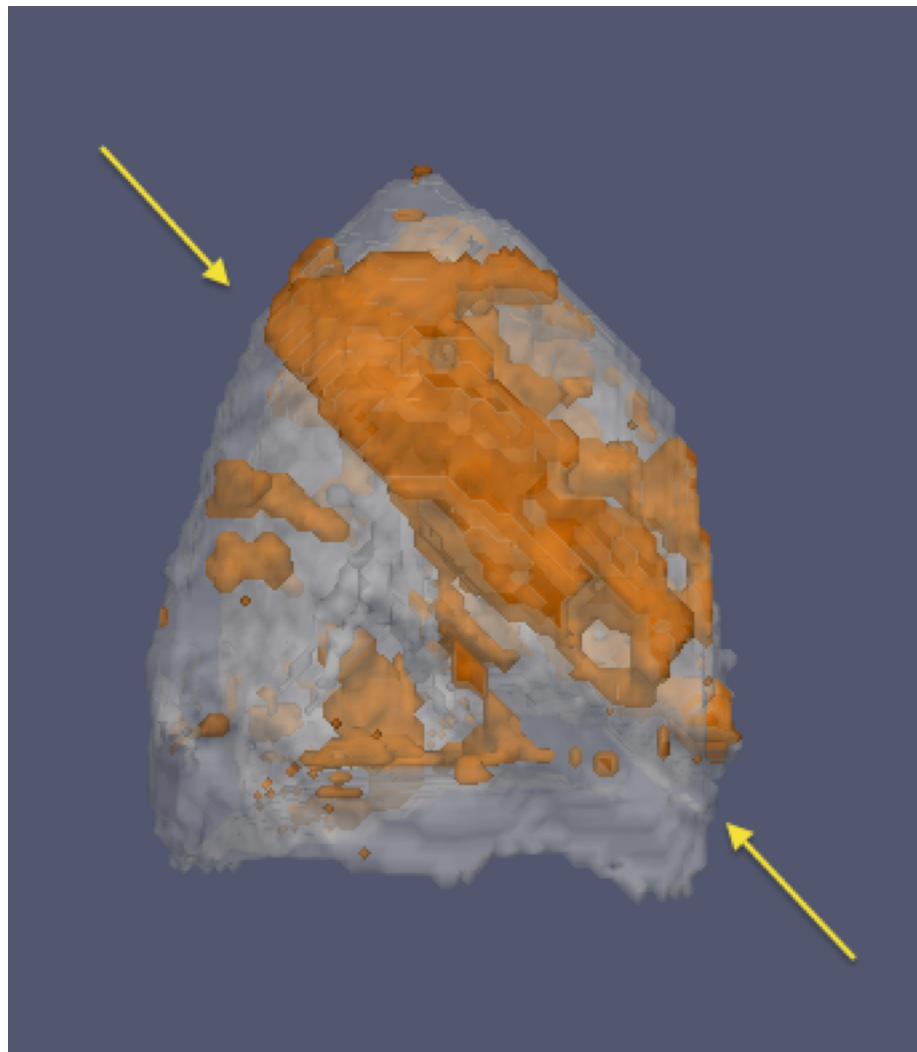


**Figure 5:** View of the left lung of patient 3, showing only positively correlated regions (i.e., regions that improved with treatment). The arrows indicate the lobar fissure, demonstrating a predominant upper lobe treatment effect.

**Table 1:** Summary statistics for the correlation volumes shown in Figure 4. Given are total volume and positively and negatively correlated subvolumes.

Subject	Volume (L)	Positively Correlated	Negatively Correlated
		Subvolume (L)	Subvolume (L)
1	3.52	0.73	0.62
2	5.56	2.95	0.46
3	4.70	1.32	0.93
4	5.05	1.76	0.55
5	3.82	1.11	0.39
6	4.60	2.11	0.32
7	4.44	1.57	0.75
8	3.86	1.58	0.32

population- or patient-specific templates enhanced the accuracy of the longitudinal analysis. Furthermore, the voxel-based longitudinal analysis technique used in this study enables voxelwise statistical regression for determining spatial correlation with expected treatment effects. This provides a new visualization and quantitative technique for exploring clinical hypotheses regarding changes in lung function.

In conclusion, these preliminary results demonstrate the potential utility of the proposed framework for providing regional information concerning such pulmonary research topics as disease progression or response to treatment. The preprocessing steps of template building, intensity normalization, inhomogeneity correction, and segmentation are all available in the ANTs distribution. Furthermore, the R statistical project, which was used to perform statistical analysis, is available at [www.r-project.org](http://www.r-project.org). Hence, the processing pipeline is readily available as an open source of information to researchers who desire to participate in and extend this work.

## **Acknowledgments**

Vertex Pharmaceuticals Incorporated provided funding for editorial support in the development of this manuscript; Edwin Thrower, PhD, provided editorial support and Dena McWain of Infusion Communications copyedited and styled the manuscript per journal requirements. Vertex Pharmaceuticals Incorporated reviewed and provided feedback on the manuscript to the authors. The authors had full editorial control of the manuscript and provided their final approval of all content.

## **Author Disclosures**

Nicholas J. Tustison:

Benjamin Contrella:

Talissa A. Altes:

Brian B. Avants:

Eduard E. de Lange:

John P. Mugler III:

## References

1. Burchfiel, C. M., Marcus, E. B., Curb, J. D., Maclean, C. J., Vollmer, W. M., Johnson, L. R., Fong, K. O., Rodriguez, B. L., Masaki, K. H., and Buist, A. S. “**Effects of Smoking and Smoking Cessation on Longitudinal Decline in Pulmonary Function**” *Am J Respir Crit Care Med* 151, no. 6 (1995): 1778–85. doi:[10.1164/ajrccm.151.6.7767520](https://doi.org/10.1164/ajrccm.151.6.7767520)
2. Kanner, R. E., Connell, J. E., Williams, D. E., and Buist, A. S. “**Effects of Randomized Assignment to a Smoking Cessation Intervention and Changes in Smoking Habits on Respiratory Symptoms in Smokers with Early Chronic Obstructive Pulmonary Disease: The Lung Health Study**” *Am J Med* 106, no. 4 (1999): 410–6.
3. Sears, M. R., Greene, J. M., Willan, A. R., Wieck, E. M., Taylor, D. R., Flannery, E. M., Cowan, J. O., Herbison, G. P., Silva, P. A., and Poulton, R. “**A Longitudinal, Population-Based, Cohort Study of Childhood Asthma Followed to Adulthood**” *N Engl J Med* 349, no. 15 (2003): 1414–22. doi:[10.1056/NEJMoa022363](https://doi.org/10.1056/NEJMoa022363)
4. Schultz, E. S., Hallberg, J., Bellander, T., Bergström, A., Bottai, M., Chiesa, F., Gustafsson, P. M., Gruzieva, O., Thunqvist, P., Pershagen, G., and Melén, E. “**Early-Life Exposure to Traffic-Related Air Pollution and Lung Function in Adolescence**” *Am J Respir Crit Care Med* 193, no. 2 (2016): 171–7. doi:[10.1164/rccm.201505-0928OC](https://doi.org/10.1164/rccm.201505-0928OC)
5. Langley, S. J., Goldthorpe, S., Craven, M., Woodcock, A., and Custovic, A. “**Relationship Between Exposure to Domestic Allergens and Bronchial Hyperresponsiveness in Non-Sensitised, Atopic Asthmatic Subjects**” *Thorax* 60, no. 1 (2005): 17–21. doi:[10.1136/thx.2004.027839](https://doi.org/10.1136/thx.2004.027839)
6. Greenwald, G. I., Tashkin, D. P., Gong, H., Simmons, M., Duann, S., Furst, D. E., and Clements, P. “**Longitudinal Changes in Lung Function and Respiratory Symptoms in Progressive Systemic Sclerosis. Prospective Study**” *Am J Med* 83, no. 1 (1987): 83–92.
7. Love, R. G. and Miller, B. G. “**Longitudinal Study of Lung Function in Coal-Miners**” *Thorax* 37, no. 3 (1982): 193–7.
8. Rom, W. N. “**Accelerated Loss of Lung Function and Alveolitis in a Longitudinal Study of Non-Smoking Individuals with Occupational Exposure to Asbestos**” *Am J Ind Med* 21, no. 6 (1992): 835–44.
9. Sherman, C. B., Xu, X., Speizer, F. E., Ferris, B. G., Jr, Weiss, S. T., and Dockery, D. W. “**Longitudinal Lung Function Decline in Subjects with Respiratory Symptoms**” *Am Rev Respir Dis* 146, no. 4 (1992):

855–9. doi:[10.1164/ajrccm/146.4.855](https://doi.org/10.1164/ajrccm/146.4.855)

10. Vestbo, J., Anderson, W., Coxson, H. O., Crim, C., Dawber, F., Edwards, L., Hagan, G., Knobil, K., Lomas, D. A., MacNee, W., Silverman, E. K., Tal-Singer, R., and ECLIPSE investigators. “**Evaluation of COPD Longitudinally to Identify Predictive Surrogate End-Points (ECLIPSE)**” *Eur Respir J* 31, no. 4 (2008): 869–73. doi:[10.1183/09031936.00111707](https://doi.org/10.1183/09031936.00111707)
11. Ohara, T., Hirai, T., Sato, S., Terada, K., Kinose, D., Haruna, A., Marumo, S., Nishioka, M., Ogawa, E., Nakano, Y., Hoshino, Y., Ito, Y., Matsumoto, H., Niimi, A., Mio, T., Chin, K., Muro, S., and Mishima, M. “**Longitudinal Study of Airway Dimensions in Chronic Obstructive Pulmonary Disease Using Computed Tomography**” *Respirology* 13, no. 3 (2008): 372–8. doi:[10.1111/j.1440-1843.2008.01269.x](https://doi.org/10.1111/j.1440-1843.2008.01269.x)
12. Dirksen, A., Dijkman, J. H., Madsen, F., Stoel, B., Hutchison, D. C., Ulrik, C. S., Skovgaard, L. T., Kok-Jensen, A., Rudolphus, A., Seersholtz, N., Vrooman, H. A., Reiber, J. H., Hansen, N. C., Heckscher, T., Viskum, K., and Stolk, J. “**A Randomized Clinical Trial of Alpha(1)-Antitrypsin Augmentation Therapy**” *Am J Respir Crit Care Med* 160, no. 5 Pt 1 (1999): 1468–72. doi:[10.1164/ajrccm.160.5.9901055](https://doi.org/10.1164/ajrccm.160.5.9901055)
13. Remy-Jardin, M., Edme, J.-L., Boulenguez, C., Remy, J., Mastora, I., and Sobaszek, A. “**Longitudinal Follow-up Study of Smoker’s Lung with Thin-Section CT in Correlation with Pulmonary Function Tests**” *Radiology* 222, no. 1 (2002): 261–70. doi:[10.1148/radiol.2221001154](https://doi.org/10.1148/radiol.2221001154)
14. Stolk, J., Ng, W. H., Bakker, M. E., Reiber, J. H. C., Rabe, K. F., Putter, H., and Stoel, B. C. “**Correlation Between Annual Change in Health Status and Computer Tomography Derived Lung Density in Subjects with Alpha1-Antitrypsin Deficiency**” *Thorax* 58, no. 12 (2003): 1027–30.
15. Parr, D. G., Sevenoaks, M., Deng, C., Stoel, B. C., and Stockley, R. A. “**Detection of Emphysema Progression in Alpha 1-Antitrypsin Deficiency Using CT Densitometry; Methodological Advances**” *Respir Res* 9, (2008): 21. doi:[10.1186/1465-9921-9-21](https://doi.org/10.1186/1465-9921-9-21)
16. Stolk, J., Putter, H., Bakker, E. M., Shaker, S. B., Parr, D. G., Piitulainen, E., Russi, E. W., Grebski, E., Dirksen, A., Stockley, R. A., Reiber, J. H. C., and Stoel, B. C. “**Progression Parameters for Emphysema: A Clinical Investigation**” *Respir Med* 101, no. 9 (2007): 1924–30. doi:[10.1016/j.rmed.2007.04.016](https://doi.org/10.1016/j.rmed.2007.04.016)
17. Tanabe, N., Muro, S., Hirai, T., Oguma, T., Terada, K., Marumo, S., Kinose, D., Ogawa, E., Hoshino, Y., and Mishima, M. “**Impact of Exacerbations on Emphysema Progression in Chronic Obstructive Pulmonary Disease**” *Am J Respir Crit Care Med* 183, no. 12 (2011): 1653–9. doi:[10.1164/rccm.201009-1535OC](https://doi.org/10.1164/rccm.201009-1535OC)
18. Soejima, K., Yamaguchi, K., Kohda, E., Takeshita, K., Ito, Y., Mastubara, H., Oguma, T., Inoue, T., Okubo, Y., Amakawa, K., Tateno, H., and Shiomi, T. “**Longitudinal Follow-up Study of Smoking-Induced Lung**

**Density Changes by High-Resolution Computed Tomography”** *Am J Respir Crit Care Med* 161, no. 4 Pt 1 (2000): 1264–73. doi:[10.1164/ajrccm.161.4.9905040](https://doi.org/10.1164/ajrccm.161.4.9905040)

19. Lange, E. E. de, Mugler, J. P., 3rd, Brookeman, J. R., Knight-Scott, J., Truwit, J. D., Teates, C. D., Daniel, T. M., Bogorad, P. L., and Cates, G. D. “**Lung Air Spaces: MR Imaging Evaluation with Hyperpolarized 3He Gas**” *Radiology* 210, no. 3 (1999): 851–7. doi:[10.1148/radiology.210.3.r99fe08851](https://doi.org/10.1148/radiology.210.3.r99fe08851)
20. Tustison, N. J., Altes, T. A., Song, G., Lange, E. E. de, Mugler, J. P., 3rd, and Gee, J. C. “**Feature Analysis of Hyperpolarized Helium-3 Pulmonary MRI: A Study of Asthmatics Versus Nonasthmatics**” *Magn Reson Med* 63, no. 6 (2010): 1448–55. doi:[10.1002/mrm.22390](https://doi.org/10.1002/mrm.22390)
21. Tustison, N. J., Avants, B. B., Flors, L., Altes, T. A., Lange, E. E. de, Mugler, J. P., 3rd, and Gee, J. C. “**Ventilation-Based Segmentation of the Lungs Using Hyperpolarized (3)He MRI**” *J Magn Reson Imaging* 34, no. 4 (2011): 831–41. doi:[10.1002/jmri.22738](https://doi.org/10.1002/jmri.22738)
22. Kirby, M., Heydarian, M., Svenningsen, S., Wheatley, A., McCormack, D. G., Etemad-Rezai, R., and Parraga, G. “**Hyperpolarized 3He Magnetic Resonance Functional Imaging Semiautomated Segmentation**” *Acad Radiol* 19, no. 2 (2012): 141–52. doi:[10.1016/j.acra.2011.10.007](https://doi.org/10.1016/j.acra.2011.10.007)
23. Ley, S., Zaporozhan, J., Morbach, A., Eberle, B., Gast, K. K., Heussel, C. P., Biedermann, A., Mayer, E., Schmiedeskamp, J., Stepniak, A., Schreiber, W. G., and Kauczor, H.-U. “**Functional Evaluation of Emphysema Using Diffusion-Weighted 3Helium-Magnetic Resonance Imaging, High-Resolution Computed Tomography, and Lung Function Tests**” *Invest Radiol* 39, no. 7 (2004): 427–34.
24. Kirby, M., Mathew, L., Wheatley, A., Santyr, G. E., McCormack, D. G., and Parraga, G. “**Chronic Obstructive Pulmonary Disease: Longitudinal Hyperpolarized (3)He MR Imaging**” *Radiology* 256, no. 1 (2010): 280–9. doi:[10.1148/radiol.10091937](https://doi.org/10.1148/radiol.10091937)
25. Collins, D. L., Neelin, P., Peters, T. M., and Evans, A. C. “**Automatic 3D Intersubject Registration of MR Volumetric Data in Standardized Talairach Space**” *J Comput Assist Tomogr* 18, no. 2 (): 192–205.
26. Smith, S. M. “**Overview of FMRI Analysis**” *Br J Radiol* 77 Spec No 2, (2004): S167–75. doi:[10.1259/bjr/33553595](https://doi.org/10.1259/bjr/33553595)
27. Altes, T., Johnson, M., III, J. M., Miller, G. W., Flors, L., Mata, J., Salinas, C., Tustison, N., Lee, P.-S., Song, T., Yen, K., Froh, D., and Botfield, M. “**The Effect of Ivacaftor, an Investigational CFTR Potentiator, on Hyperpolarized Noble Gas Magnetic Resonance Imaging in Subjects with Cystic Fibrosis Who Have the G551D-CFTR Mutation**” (2012): A2814–A2814.
28. Nyúl, L. G., Udupa, J. K., and Zhang, X. “**New Variants of a Method of MRI Scale Standardization**”

*IEEE Trans Med Imaging* 19, no. 2 (2000): 143–50. doi:[10.1109/42.836373](https://doi.org/10.1109/42.836373)

29. Avants, B. B., Yushkevich, P., Pluta, J., Minkoff, D., Korczykowski, M., Detre, J., and Gee, J. C. “**The Optimal Template Effect in Hippocampus Studies of Diseased Populations**” *Neuroimage* 49, no. 3 (2010): 2457–66. doi:[10.1016/j.neuroimage.2009.09.062](https://doi.org/10.1016/j.neuroimage.2009.09.062)

30. Tustison, N. J., Shrinidhi, K. L., Wintermark, M., Durst, C. R., Kandel, B. M., Gee, J. C., Grossman, M. C., and Avants, B. B. “**Optimal Symmetric Multimodal Templates and Concatenated Random Forests for Supervised Brain Tumor Segmentation (Simplified) with ANTsR**” *Neuroinformatics* 13, no. 2 (2015): 209–25. doi:[10.1007/s12021-014-9245-2](https://doi.org/10.1007/s12021-014-9245-2)